

Characterizing Shortest Paths in Road Systems Modeled as Manhattan Poisson Line Processes

Vishnu Vardhan Chetlur, Harpreet S. Dhillon, Carl P. Dettmann

Abstract—In this paper, we model a transportation network by a Cox process where the road systems are modeled by a Manhattan Poisson line process (MPLP) and the locations of vehicles and desired destination sites, such as gas stations or charging stations, referred to as *facilities*, are modeled by independent 1D Poisson point processes (PPP) on each of the lines. For this setup, we characterize the length of the shortest path between a typical vehicular user and its nearest facility that can be reached by traveling along the streets. For a typical vehicular user starting from an intersection, we derive the closed-form expression for the exact cumulative distribution function (CDF) of the length of the shortest path to its nearest facility in the sense of path distance. Building on this result, we derive an upper bound and a remarkably accurate but approximate lower bound on the CDF of the shortest path distance to the nearest facility for a typical vehicle starting from an arbitrary position on a road. These results can be interpreted as nearest-neighbor distance distributions (in terms of the path distance) for this Cox process, which is a key technical contribution of this paper. In addition to these analytical results, we also present a simulation procedure to characterize any distance-dependent cost metric between a typical vehicular user and its nearest facility in the sense of path distance using graphical interpretation of the spatial model. We also discuss extension of this work to other cost metrics and possible applications to the areas of urban planning, personnel deployment and wireless communication.

Index Terms—Stochastic geometry, Manhattan Poisson line process, Cox process, path distance, shortest path.

I. INTRODUCTION

Transportation systems have been studied by researchers from various fields such as geography, operations research, and recently, complex network theory [1], [2]. It is quite intuitive to model transportation networks as graphs where various sites are modeled as nodes of the graph and the routes between them are represented by the edges of the graph [3]. Several spatial network models have been proposed in the literature ranging from simple proximity graphs where the edges of the graph are defined by a deterministic set of rules to more sophisticated models where the probability of an edge between a pair of nodes is a function of position of the nodes [4], [5]. While these network models are useful in studying the topological properties of the network such as connectivity, closeness and centrality, they do not capture some of the geometric aspects such as the continuity of street segments [2], [6]. So, instead

of taking a node-centric approach where the streets were considered as links between various sites in a city, we visualize these sites to be located on an underlying street network. Although relatively sparse, there have been a few works in the stochastic geometry literature, where street networks were modeled by a set of random lines, referred to as a *line process* in the 2D Euclidean space [7]–[9]. A well-known canonical line process model in the literature is the Poisson line process (PLP) [10], [11]. Inspired by the grid-like structure of road layouts of many cities, e.g., New York, as well as the nature of mathematical problems to be studied in this paper, we limit our attention to a special case of PLP called *Manhattan Poisson line process (MPLP)* in this paper [12], [13]. Further, the locations of vehicles, and the locations of various places such as gas stations or charging stations for electric vehicles, which will henceforth be referred to as simply *facilities*, are modeled as 1D Poisson point process (PPP) on each line of the line process, thereby forming a doubly stochastic Poisson point process or Cox process [14], [15]. To the best of our knowledge, this is the first paper to employ Cox process driven by MPLP to study urban road transportation systems. So, the characterization of even some of the basic properties such as the length of the shortest path between neighboring points is still an open problem and is the main focus of this paper. In particular, we derive the distribution of the length of the shortest path between an arbitrarily chosen vehicle and its nearest facility in the sense of path distance.

A. Prior Art

We will first review some of the well-known network models in the literature. One of the first and most important network models is the Erdős-Rényi (ER) graph characterized by the number of vertices and the probability of an edge between any two vertices in the graph [16], [17]. However, the small clustering coefficient of the ER graphs does not agree with the empirical data from many real-world networks. In [18], Barabási and Albert proposed a model that exhibits preferential connectivity, and has improved clustering coefficient and scale-free properties. Spatial networks, in which vertices have a physical location and most links are over short distances, retain a large clustering coefficient but usually without extremely high degree nodes. Examples include the Watts-Strogatz small-world network [19] and the Hammersley network proposed by Aldous [4], [20]. In the latter, the vertices are defined by an infinite PPP and each vertex has exactly four edges. However, one of the major limitations of most of these network models is that they do not accurately capture the

V. V. Chetlur and H. S. Dhillon are with Wireless@VT, Department of ECE, Virginia Tech, Blacksburg, VA (email: {vishnu, dhillion}@vt.edu). C. P. Dettmann is with School of Mathematics, University of Bristol, UK (email: carl.dettmann@bristol.ac.uk). The support of the US National Science Foundation (Grant IIS-1633363) and UK Engineering and Physical Sciences Research Council (Grant EP/N002458/1) is gratefully acknowledged. Manuscript updated: May 11, 2022.

continuity of streets, especially in modeling urban street networks. Therefore, we model an urban transportation network by a Cox process driven by a MPLP. As will be evident from the technical discussions, such models are particularly well-suited for the statistical analysis of the geometric properties, such as path lengths.

The idea of using a PLP to model road systems was first proposed by Baccelli in [7] to study the handover rate in cellular networks. While there have been other models where the roads are modeled by the edges of a Poisson Voronoi tessellation (PVT) or Poisson Delaunay tessellation (PDT), PLP is often preferred due to its analytical tractability [21]–[23]. This spatial model was later employed in several works in the area of wireless communications, particularly vehicular networks, where the locations of transmitters and receivers were modeled by a Cox process driven by a PLP or MPLP [9], [12], [21], [24]–[26]. However, only Euclidean distances between the points of the Cox process were considered in all these works. Nonetheless, there have been a few works in the literature where the distance measured along the line segments of the path was considered. In [13], the authors have computed the path-loss for a signal propagating along the streets of an urban network modeled by a MPLP. In [8], the authors have modeled a two-tier wired network by a Cox process driven by a PLP and characterized the mean shortest path along the lines between a component and its nearest neighbor in the Euclidean distance sense. Therefore, this is the first paper to derive the distribution of the length of the shortest path between a typical point and its nearest neighbor in the sense of path distance in a Cox process driven by a MPLP. More technical details about our contribution are provided next.

B. Contributions

In this paper, we model the random spatial layout of roads by a MPLP. We further model the random locations of vehicles and facilities on each road as independent 1D PPPs on each line of the MPLP. For this setup, we characterize the least cost path to arrive at a facility for a typical vehicular user, which is an arbitrarily chosen vehicle in the spatial model (point process of vehicles). Owing to its analytical tractability, the cost metric that we mainly focus on is the length of the path traveled by the typical vehicular user (and its variants, such as monotonic functions of this distance). We also present techniques to compute other cost metrics such as time of travel through Monte-Carlo simulations. We then discuss the insights that we gain from the analytical results and also possible extensions of these results to various applications. More technical details are discussed next.

Distance Distributions. We derive the cumulative distribution function (CDF) of the length of the shortest path from a typical vehicular user to its nearest facility in the sense of path distance. It is important to note that the closest facility to the typical vehicle in the sense of Euclidean distance is not necessarily the one with the least path length. For a typical vehicular user located at an intersection, we derive the exact closed-form expression for the CDF of the shortest path distance. Building on this result, we propose an upper

bound on the CDF of the shortest path distance for a typical vehicular user located at some arbitrary position on the line and its nearest facility in the sense of path distance. We also derive a remarkably tight but approximate lower bound on the CDF of this distance.

Simulation Techniques. Complementary to the analytical characterizations, we also present a simulation method to compute any distance-based cost metric such as travel time or fuel consumed by the typical vehicular user to reach the nearest facility. The graphical interpretation of the spatial model enables the application of some well-known algorithms in the literature that would be useful in reducing the run-time of simulations.

Insights and Applications. We demonstrate the utility of our results in addressing some statistical problems in the areas of transportation, infrastructure planning, personnel deployment and wireless communication. Using our analytical results, one can easily determine the minimum density of facilities that is necessary to ensure that the shortest path distance for a typical vehicular user to its nearest facility in the sense of path distance is smaller than a desired value with some probability. We can also gain such insights for travel time which is a critical metric for estimating the response time of medical help or police personnel in emergency situations. In wireless communications, the analytical techniques developed in this paper could be useful in characterizing the received signal power in millimeter wave (mmWave) frequency communications where the dominant signal could be the one that travels along the streets due to high penetration losses through buildings.

II. LINE PROCESS PRELIMINARIES

Since the spatial model considered in the paper involves line processes, we introduce this topic briefly in this section. While we discuss only those aspects of line processes that are necessary for this paper, a detailed account of the theory can be found in [10].

Line process. Simply put, a line process is just a random collection of lines. In order to define it more formally, first observe that any undirected line L in \mathbb{R}^2 can be uniquely parameterized by its signed perpendicular distance ρ from the origin $o \equiv (0, 0)$ and the angle θ subtended by the line with respect to the positive x -axis in counter clockwise direction, as shown in Fig. 1. The sign of ρ is negative if the origin is to the right or above the line. Thus, the pair of parameters ρ and θ can be represented as the coordinates of a point on the half-cylinder $\mathcal{C} \equiv [0, \pi) \times \mathbb{R}$, which is termed as the *representation space*, as illustrated in Fig. 2. Thus, a random collection of lines in \mathbb{R}^2 can be constructed from a set of points on \mathcal{C} . Such a set of lines generated by a Poisson point process (PPP) on \mathcal{C} is called a Poisson line process (PLP).

As we mentioned earlier, we limit our discussion to a special case of PLP called MPLP in which the grid-like structure of lines resembles that of road networks in many cities. Also, due to its analytical tractability, this model has been widely used for spatial modeling of the road layouts in the wireless communications community, which served as the initial motivation behind this work [13], [27]. In fact, the

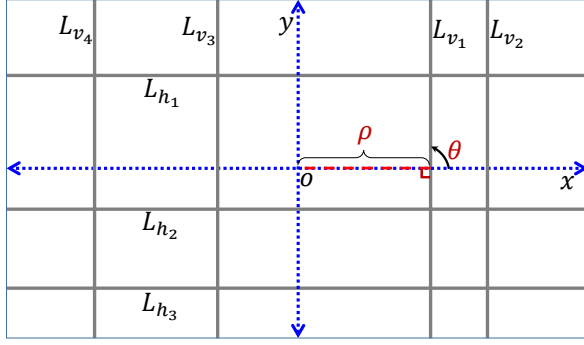


Fig. 1: Illustration of Manhattan Poisson line process in two-dimensional plane \mathbb{R}^2 .

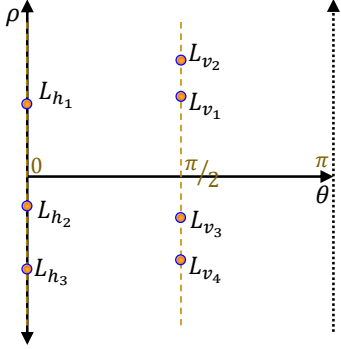


Fig. 2: Illustration of a point process in representation space $\mathcal{C} \equiv [0, \pi) \times \mathbb{R}$.

models used by the wireless standardization bodies, such as the third generation partnership project (3GPP), are simple variants or special instances of this model [28]. In MPLP, the orientations of the lines are restricted to $\{0, \pi/2\}$, thereby obtaining a set of horizontal and vertical lines in \mathbb{R}^2 . Thus, the MPLP Φ_l in \mathbb{R}^2 can be constructed from two independent 1D PPPs Ψ_0 , and $\Psi_{\pi/2}$ along the lines $\theta = 0$, and $\theta = \pi/2$, respectively, in the representation space \mathcal{C} . Alternatively, one can construct a MPLP by first populating points along the x and y -axes in \mathbb{R}^2 according to independent 1D PPPs Ξ_x and Ξ_y and drawing vertical and horizontal lines through those points, respectively. This interpretation is useful in visualizing some of the basic properties of MPLP which will be discussed next. In this paper, we will mainly follow this interpretation for the ease of clarity and exposition.

Stationarity. Analogous to a point process, a line process Φ_l is stationary if the distribution of lines is invariant to any translation $T_{(t,\beta)}$, which corresponds to the translation of the origin by a distance t in a direction that makes an angle β with respect to positive x -axis in counter clockwise direction. Upon applying a translation $T_{(t,\beta)}$, the representation of a line L in \mathcal{C} changes from (ρ, θ) to $(\rho + t \sin(\theta - \beta), \theta)$. Therefore, a MPLP Φ_l is stationary if the 1D PPPs Ψ_0 , and $\Psi_{\pi/2}$ are stationary or alternatively, Ξ_x and Ξ_y are stationary.

Line density. The line density of a line process is defined as the mean line length per unit area. The relationship between the line density and the density of the corresponding point process is given by the following Lemma.

Lemma 1. For a stationary MPLP Φ_l constructed from independent and homogeneous 1D PPPs Ξ_x and Ξ_y , each with density λ_l , the line density μ_l is given by $\mu_l = 2\lambda_l$.

Proof: Let us consider a ball of radius d centered at the origin $b(o, d)$. We denote the set of horizontal and vertical lines of Φ_l by Φ_{lh} and Φ_{lv} , respectively. The line density μ_l can now be computed as

$$\begin{aligned} \mu_l &= \frac{1}{\pi d^2} \mathbb{E} \left[\sum_{l \in \Phi_l} \nu_1(l \cap b(o, d)) \right] \\ &= \frac{1}{\pi d^2} \mathbb{E} \left[\sum_{l_h \in \Phi_{lh}} \nu_1(l_h \cap b(o, d)) + \sum_{l_v \in \Phi_{lv}} \nu_1(l_v \cap b(o, d)) \right] \\ &= \frac{1}{\pi d^2} \mathbb{E} \left[\sum_{\substack{\rho_x \in \Xi_x: \\ \rho_x \leq d}} 2\sqrt{d^2 - \rho_x^2} \right] + \frac{1}{\pi d^2} \mathbb{E} \left[\sum_{\substack{\rho_y \in \Xi_y: \\ \rho_y \leq d}} 2\sqrt{d^2 - \rho_y^2} \right] \\ &\stackrel{(a)}{=} \frac{1}{\pi d^2} (\lambda_l 2) \left[\int_0^d 2\sqrt{d^2 - \rho_x^2} d\rho_x + \int_0^d 2\sqrt{d^2 - \rho_y^2} d\rho_y \right] \\ &= 2\lambda_l, \end{aligned}$$

where $\nu_1(\cdot)$ denotes the one dimensional Lebesgue measure and (a) follows from Campbell's theorem for sums over stationary 1D PPPs Ξ_x and Ξ_y . ■

Lines intersecting a region. For a stationary MPLP Φ_l with line density μ_l , the number of horizontal and vertical lines that intersect a convex region $\mathcal{K} \subseteq \mathbb{R}^2$ are Poisson distributed with means $\mu_l \nu_1(\mathcal{K}_y)/2$ and $\mu_l \nu_1(\mathcal{K}_x)/2$, respectively, where \mathcal{K}_x and \mathcal{K}_y denote the projection of \mathcal{K} onto x and y axis.

III. SYSTEM MODEL

A. Spatial Modeling

We model the spatial layout of a system of roads by a stationary MPLP $\Phi_l \equiv \{L_{h_1}, L_{h_2}, \dots, L_{v_1}, L_{v_2}, \dots\}$ in \mathbb{R}^2 in which the vertical and horizontal lines are generated by independent homogeneous 1D PPPs Ξ_x and Ξ_y , each having density λ_l . We denote the set of horizontal and vertical lines by $\Phi_{lh} \equiv \{L_{h_1}, L_{h_2}, \dots\}$ and $\Phi_{lv} \equiv \{L_{v_1}, L_{v_2}, \dots\}$, respectively. We model the locations of vehicular users on each line by a 1D PPP with density λ_v . Thus, the locations of vehicular users in \mathbb{R}^2 form a Cox process Φ_v driven by the MPLP Φ_l . As discussed already, some models used in industry can be argued to be special cases or variants of this model [28]. Further, we model the locations of the facilities of the desired type (which could be gas stations or charging stations for electric vehicles) on each line by a 1D PPP with density λ_c thereby forming a Cox process Φ_c , as illustrated in Fig. 3. Both the Cox processes Φ_c and Φ_v driven by the stationary MPLP Φ_l are stationary [12], [29]. We will refer to an arbitrarily chosen vehicular user in the point process Φ_v as a typical vehicular user. We will consider two types of typical vehicular users in this paper: (i) *typical intersection user* located at the intersection of a horizontal and vertical line, and (ii) *typical general user* located at some arbitrary position on a line.

Without loss of generality, we place the typical vehicular user at the origin o owing to the stationarity of Φ_v . Thus,

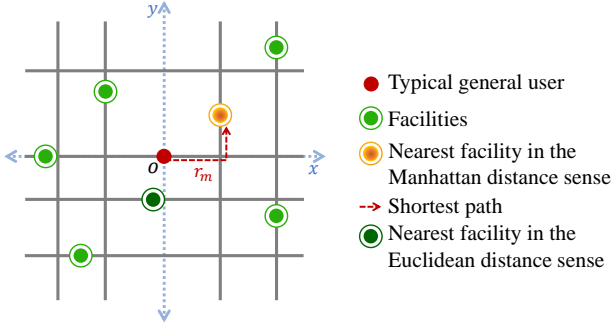


Fig. 3: Illustration of the system model.

a typical intersection user is located at the intersection of a horizontal line L_x and a vertical line L_y , which are aligned along the x and y -axes, respectively. Therefore, under this conditioning (more formally, under *Palm probability*), the resulting line process is $\Phi_{l_0, \text{int}} = \Phi_l \cup \{L_x, L_y\}$, which is a consequence of the Slivnyak's Theorem [14], [29]. Consequently, under Palm probability, the translated point process $\Phi_{v_0, \text{int}}$ can be interpreted as the superposition of the point process Φ_v , two 1D PPPs each with density λ_v along the lines L_x and L_y , and an atom at the origin [9], [25]. Similarly, since the point process Φ_c is also driven by the same MPLP Φ_l , the translated point process $\Phi_{c_0, \text{int}}$ is the superposition of Φ_c and two independent 1D PPPs each with density λ_c along L_x and L_y .

In case of a typical general user, without loss of generality, we assume that it is located on a horizontal line of the MPLP Φ_l . Upon conditioning on the location of the typical general user at the origin and using the same argument as the typical intersection user, the resulting line process is $\Phi_{l_0, \text{gen}} = \Phi_l \cup \{L_x\}$. Thus, the translated point process $\Phi_{v_0, \text{gen}}$ can be interpreted as the superposition of the point process Φ_v , an independent 1D PPP with density λ_v on the line L_x aligned along the x -axis with an atom at the origin. Similarly, the translated point process $\Phi_{c_0, \text{gen}}$ in this case is the superposition of the point process Φ_c and a 1D PPP with density λ_c on L_x .

We denote the number of horizontal and vertical lines that intersect a region $\mathcal{A} \subset \mathbb{R}^2$ by $N_h(\mathcal{A})$ and $N_v(\mathcal{A})$, respectively. We denote the number of points in the set \mathcal{A} by $N_p(\mathcal{A})$. In this paper, we will denote the random variables by upper case letters and their corresponding realizations by lower case letters. For example, W denotes a random variable, whereas w denotes its realization. We defer the definition of other variables to later sections of the paper for better readability.

B. Cost Metrics

Our goal is to characterize the minimum cost involved in traveling to a facility for a typical vehicular user. For instance, consider a typical vehicular user that is interested in going to the *nearest* gas station. Generally speaking, our goal in this paper is to statistically characterize the cost of traveling from the current location of this vehicle to its nearest gas station. The main metric of interest for us in this paper is the *path distance* (and its variants, such as monotone functions of the

path distance). In order to be concrete, we formally define path distance next.

Definition 1. (Path distance.) *The path distance between two points $\mathbf{a}(x_1, y_1)$ and $\mathbf{b}(x_2, y_2)$ is defined as the sum of lengths of the line segments that constitute a path P from \mathbf{a} to \mathbf{b} and is denoted by $\ell(\mathbf{a}, \mathbf{b})$.*

Therefore, in order to minimize the cost of travel, the typical vehicular user must travel to its nearest facility in the sense of path distance. Note that this is true for any cost metric which is a monotonically decreasing function of the path distance. Thus, for such metrics, the minimum cost of travel will correspond to the shortest path distance between the typical vehicular user and its nearest facility in the sense of path distance and is denoted by R_m . Mathematically, it can be expressed as $R_m = \min_{x_i \in \Phi_{c_0, \text{int}}} \ell(o, x_i)$ for a typical intersection user and $R_m = \min_{x_i \in \Phi_{c_0, \text{gen}}} \ell(o, x_i)$ for a typical general user. We will also discuss a few other cost metrics, such as travel time, in Section V-C.

IV. ANALYTICAL RESULTS

In this section, we will characterize the distribution of the minimum path distance R_m . First, we will determine the exact CDF of R_m for a typical intersection user. Building on this result, we will provide an upper bound and an approximate lower bound for the CDF of R_m for a typical general user.

A. Typical Intersection User

For a typical intersection user located at the origin, the length of the shortest path to any point located at (x_i, y_i) is simply given by $z_i = |x_i| + |y_i|$, which is nothing but the first order Minkowski distance of the point from the origin. If the closest facility to the typical intersection vehicle (in the sense of path distance) is at a distance r_m , then there can not be any facility at a location (x, y) in \mathbb{R}^2 such that $|x| + |y| < r_m$. Thus, as depicted in Fig. 4, we obtain an exclusion zone B_0 formed by the intersection of the half-planes $x + y < r_m$, $-x + y < r_m$, $-x - y < r_m$, and $x - y < r_m$. There can be no facilities on any of the line segments inside the square region B_0 . In addition to L_x and L_y , we know that there are a random number of lines that intersect the region B_0 . From the construction of MPLP, it follows that the number of horizontal and vertical lines that intersect B_0 are Poisson distributed with mean $\lambda_l 2r_m$. For a horizontal line located at a distance $y_l < r_m$ from the origin, the length of the line segment inside B_0 is given by $2r_m - 2y_l$. Similarly, for a vertical line at a distance $x_l < r_m$ from the origin, the length of the line segment inside B_0 is $2r_m - 2x_l$. Using these properties, we will now derive a closed-form expression for the CDF of the shortest path distance from a typical intersection user to its nearest facility in the sense of path distance in the following theorem.

Theorem 1. *The CDF of the shortest path distance from a typical intersection vehicle to its nearest facility in the sense of path distance is*

$$F_{R_m}(r_m)$$

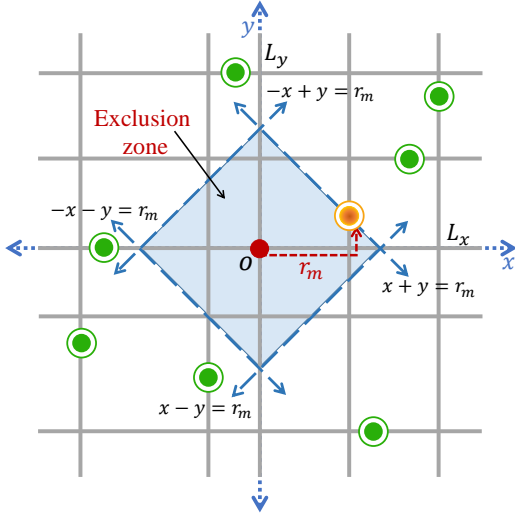


Fig. 4: Illustration of the exclusion zone for a typical intersection user.

$$= 1 - \exp \left[-4\lambda_c r_m - 4\lambda_l r_m + \frac{2\lambda_l}{\lambda_c} (1 - e^{-2\lambda_c r_m}) \right]. \quad (1)$$

Proof: See Appendix A. ■

B. Typical General User

In this subsection, we propose an upper bound and an approximate lower bound for the CDF of R_m for a typical general user located at the origin on the horizontal line L_x aligned along the x -axis.

Remark 1. The key difference between the spatial setup of the typical general user and that of the typical intersection user is that there does not exist a line L_y along the y -axis in case of a typical general user. More precisely, the point process is now viewed under the reduced Palm distribution of Ξ_x and Palm distribution of Ξ_y . This interpretation will allow us to derive an upper bound for the distribution of R_m for the typical general user using the results derived for the typical intersection user in Theorem 1.

1) *Upper Bound:* As mentioned in Remark 1, there is no vertical line at the origin for a typical general user. Consequently, a typical general user can move only along the direction of either positive or negative x -axis on the line L_x , whereas a typical intersection user could move in any of the four directions from the origin. Therefore, unlike the case of the typical intersection user where the length of the shortest path to a facility was equal to the first order Minkowski distance, the distance to some facilities from the origin in case of the typical general user is greater than their first order Minkowski distance, as illustrated in Fig. 5. Thus, in this case, the first order Minkowski distance of the nearest facility from the origin is a lower bound on R_m . Therefore, using the result derived in Theorem 1, we present a closed-form upper bound on the CDF of R_m in the following proposition.

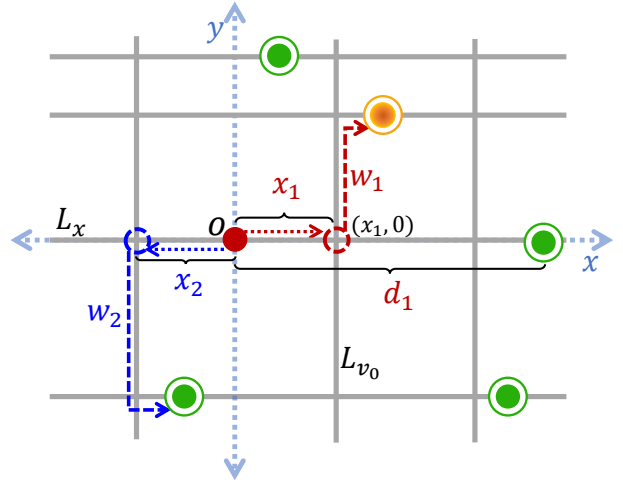


Fig. 5: Illustration of the shortest paths for a typical general user.

Proposition 1. For a typical general user, the CDF of R_m is upper bounded by

$$F_{R_m}(r_m) \leq 1 - \exp \left[-2\lambda_c r_m - 4\lambda_l r_m + \frac{2\lambda_l}{\lambda_c} (1 - e^{-2\lambda_c r_m}) \right]. \quad (2)$$

Proof: This result can be directly derived from the expression in Theorem 1 by deleting the line L_y . This means that we remove the terms corresponding to the vertical line L_y aligned along the y -axis. Specifically, we remove the term $\mathbb{P}(N_p(L_y \cap B_0) = 0)$ in step (a) and the corresponding expressions in the subsequent steps in the proof of Theorem 1 to obtain the final expression. ■

As will be shown in the later sections of the paper, this upper bound is reasonable but not extremely tight. We will propose a much tighter lower bound for the CDF of R_m next.

2) *Approximate Lower Bound:* We define a random variable R_1 as the shortest path distance from the origin to the nearest facility located to the right of y -axis upon starting in the direction of positive x -axis. Similarly, we define R_2 as the shortest path distance to the nearest facility located to the left of the y -axis when the typical general user starts in the direction of negative x -axis. Thus, the overall shortest path distance to a facility from the origin can be written as $R_m \leq \min\{R_i\}_{i=1,2}$. The inequality is due to the fact that for some facilities to the right and left of y -axis, the shortest path from the origin would be the one that starts along the direction of negative and positive x -axis from the origin, respectively, as illustrated in Fig. 6. So, in such scenarios, R_1 or R_2 would be an upper bound on the shortest path distances to those facilities. Therefore, the CDF of R_m would be bounded from below by the CDF of $\min\{R_i\}_{i=1,2}$.

When the typical general user starts in any of the two directions, there are two possible events: (i) the user could reach an intersection before arriving at any facility, and (ii) the user could arrive at a facility on the same road before

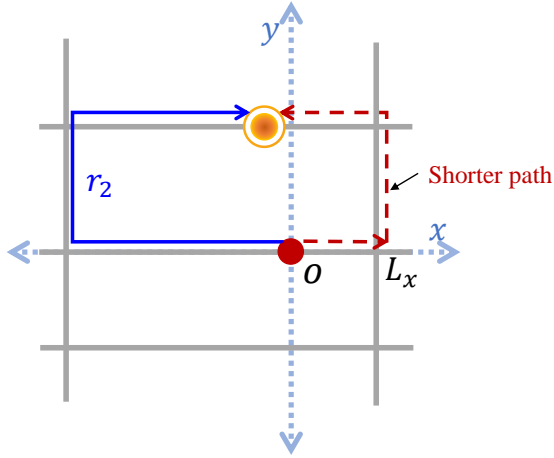


Fig. 6: Illustration of the scenario in which the shortest path to a facility to the left of the y -axis is the one that starts in the direction of positive x -axis.

reaching an intersection. Therefore, R_i can be mathematically written as

$$R_i = \begin{cases} X_i + W_i, & \mathcal{E}_{0,i} \text{ occurs,} \\ D_i, & \mathcal{E}_{1,i} \text{ occurs.} \end{cases} \quad (3)$$

We now define all the random variables appearing in (3). For notational consistency, we denote the scenario in which the typical general user starts in the positive x -axis direction by the subscript $i = 1$ and the scenario in which the user starts in the negative x -axis direction by the subscript $i = 2$. The event in which the typical general user would reach an intersection before arriving at a facility is denoted by $\mathcal{E}_{0,i}$ and its complementary event is denoted by $\mathcal{E}_{1,i}$. D_i denotes the distance to the first facility from the origin and X_i denotes the distance to the first intersection from the origin in the direction of travel, as shown in Fig. 5. W_1 and W_2 denote the shortest first order Minkowski distance from the intersection to facilities located to the right and left of the y -axis, respectively.

As the locations of facilities on each line follows a 1D PPP with mean λ_c , the distance D_i is exponentially distributed with mean λ_c^{-1} . Thus, the CDF and PDF of D_i are

$$\text{CDF: } F_{D_i}(d_i) = 1 - \exp(-\lambda_c d_i), \quad (4)$$

$$\text{PDF: } f_{D_i}(d_i) = \lambda_c \exp(-\lambda_c d_i). \quad (5)$$

Since the points at which the vertical lines cross the x -axis form a 1D PPP with density λ_l , the distance X_i also follows an exponential distribution with mean λ_l^{-1} . Thus, the CDF and PDF of X_i are

$$\text{CDF: } F_{X_i}(x_i) = 1 - \exp(-\lambda_l x_i), \quad (6)$$

$$\text{PDF: } f_{X_i}(x_i) = \lambda_l \exp(-\lambda_l x_i). \quad (7)$$

We will now focus on computing the distribution of R_i . Note that R_1 and R_2 are identically distributed due to symmetry about the y -axis. Therefore, it is sufficient to derive the marginal distribution of one of them. Without loss of generality, let us consider R_1 . Since R_1 is defined separately

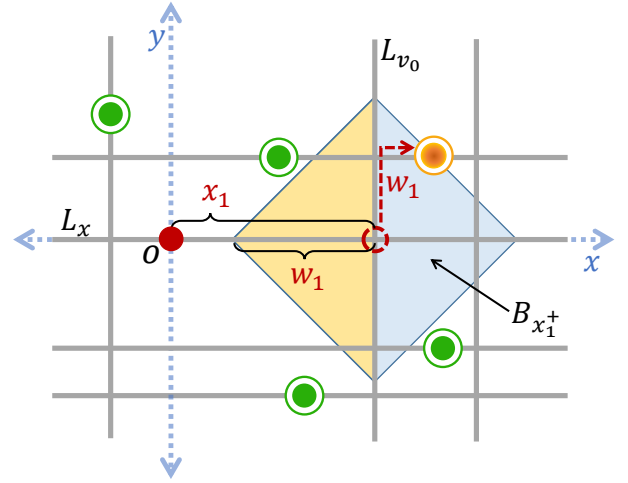


Fig. 7: Illustration of the exclusion zone for the case $w_1 < x_1$.

for the events $\mathcal{E}_{0,1}$ and $\mathcal{E}_{1,1}$, we will derive the CDF of R_1 conditioned on these events and then obtain the overall CDF using law of total probability. We will begin by deriving the probability of occurrence of the events $\mathcal{E}_{0,1}$ and $\mathcal{E}_{1,1}$ in the following Lemma.

Lemma 2. *The probability of occurrence of the events $\mathcal{E}_{0,1}$ and $\mathcal{E}_{1,1}$ are given by*

$$\mathbb{P}(\mathcal{E}_{0,1}) = \frac{\lambda_l}{\lambda_l + \lambda_c} \text{ and } \mathbb{P}(\mathcal{E}_{1,1}) = \frac{\lambda_c}{\lambda_l + \lambda_c}. \quad (8)$$

Proof: The probability of the event $\mathcal{E}_{0,1}$ can be calculated as

$$\begin{aligned} \mathbb{P}(\mathcal{E}_{0,1}) &= \mathbb{P}(D_1 > X_1) = \mathbb{E}_{X_1} [\mathbb{P}(D_1 > x_1 | X_1)] \\ &= \int_0^\infty (1 - F_{D_1}(x_1)) f_{X_1}(x_1) dx_1 \\ &= \int_0^\infty e^{-\lambda_c x_1} \lambda_l e^{-\lambda_l x_1} dx_1 \\ &= \frac{\lambda_l}{\lambda_l + \lambda_c}. \end{aligned}$$

Since the events $\mathcal{E}_{0,1}$ and $\mathcal{E}_{1,1}$ are complementary, the probability of occurrence of $\mathcal{E}_{1,1}$ can be calculated as $\mathbb{P}(\mathcal{E}_{1,1}) = 1 - \mathbb{P}(\mathcal{E}_{0,1})$. This completes the proof. ■

We will focus on the computation of the CDF of W_1 conditioned on the event $\mathcal{E}_{0,1}$ next. The conditioning on $\mathcal{E}_{0,1}$ implies that there does not exist any facility between the origin and the intersection. This additional information about the distribution of facilities in the interval $[0, X_1)$ on L_x must be included in the computation of the conditional CDF of W_1 . Since the distance X_1 is random, we will derive the intermediate results by additionally conditioning on X_1 and we will take expectation over X_1 in the final step in the computation of the marginal CDF of R_1 . Similar to the procedure followed in the derivation of Theorem 1, we will consider an exclusion zone B formed by the intersection of the half-planes $(x - x_1) + y < w_1$, $-(x - x_1) + y < w_1$, $-(x - x_1) - y < w_1$, $(x - x_1) - y < w_1$, and $x > 0$. Note that the shape of the exclusion region B depends on the values

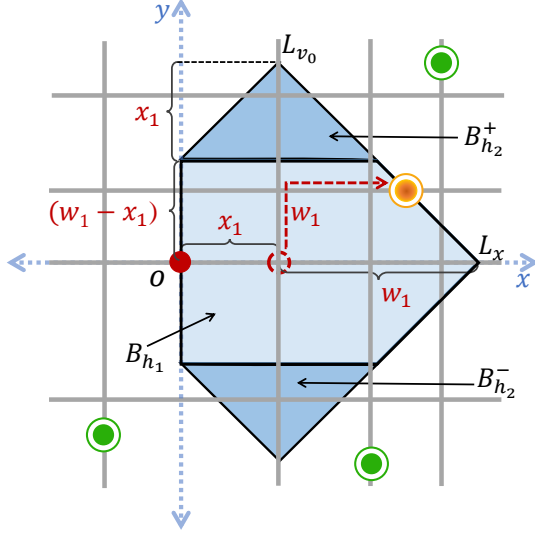


Fig. 8: Illustration of the exclusion zone for the case $w_1 \geq x_1$.

of w_1 with respect to x_1 . While B is a square for $w_1 < x_1$, it is a pentagon for $w_1 \geq x_1$, as shown in Figs. 7 and 8, respectively. So, we will derive the conditional CDF of W_1 for the two cases $w_1 < x_1$ and $w_1 \geq x_1$ separately. We know that there can not be any facility on any of the line segments inside B . In addition to L_x , there exists a random number of horizontal lines above and below the line L_x that intersect the region B . Likewise, in addition to the vertical line of the intersection L_{v_0} , there exists a random number of vertical lines that intersect the region B . However, conditioned on the event $\mathcal{E}_{0,1}$, the distribution of vertical lines to the left of L_{v_0} is not the same as the distribution of lines to the right of L_{v_0} . Since the first intersection to the right of the origin is at a distance x_1 , there can not be any vertical line that intersects L_x in the interval $[0, x_1)$, as shown in Fig. 7. So, we just need to focus on the set of vertical lines that intersect the region $B_{x_1^+} = B \cap \{x > x_1\}$. We will now derive a closed form expression for the conditional CDF of W_1 in the following Lemma.

Lemma 3. *The CDF of W_1 conditioned on $\mathcal{E}_{0,1}$ and X_1 is given by*

$$F_{W_1}(w_1|\mathcal{E}_{0,1}, x_1) = \begin{cases} F_{W_1,1}(w_1|\mathcal{E}_{0,1}, x_1), & 0 \leq w_1 < x_1, \\ F_{W_1,2}(w_1|\mathcal{E}_{0,1}, x_1), & w_1 \geq x_1, \end{cases} \quad (9)$$

where

$$F_{W_1,1}(w_1|\mathcal{E}_{0,1}, x_1) = 1 - \exp \left[-3\lambda_c w_1 - 3\lambda_l w_1 + \frac{3\lambda_l}{2\lambda_c} (1 - e^{-2\lambda_c w_1}) \right], \quad (10)$$

and

$$F_{W_1,2}(w_1|\mathcal{E}_{0,1}, x_1) = 1 - \exp \left[-3(\lambda_c + \lambda_l)w_1 - \lambda_c x_1 \right]$$

$$+ \frac{\lambda_l}{2\lambda_c} (3 + 2e^{-2\lambda_c x_1} - e^{-2\lambda_c w_1} - 4e^{-\lambda_c(x_1+w_1)}) \Big]. \quad (11)$$

Proof: See Appendix B. ■

Having determined all the components required to compute the CDF of R_1 conditioned on $\mathcal{E}_{0,1}$, we will now proceed to the derivation of CDF of R_1 conditioned on $\mathcal{E}_{1,1}$ in the following Lemma.

Lemma 4. *Conditioned on the event $\mathcal{E}_{1,1}$, the CDF of R_1 is given by*

$$F_{R_1}(r_1|\mathcal{E}_{1,1}) = 1 - \exp(-(\lambda_l + \lambda_c)r_1). \quad (12)$$

Proof: The conditional CDF of R_1 can be computed as

$$\begin{aligned} F_{R_1}(r_1|\mathcal{E}_{1,1}) &= \mathbb{P}(R_1 < r_1|\mathcal{E}_{1,1}) \\ &= 1 - \frac{\mathbb{P}(R_1 > r_1, \mathcal{E}_{1,1})}{\mathbb{P}(\mathcal{E}_{1,1})} \\ &\stackrel{(a)}{=} 1 - \frac{\mathbb{P}(D_1 > r_1, D_1 < X_1)}{\mathbb{P}(\mathcal{E}_{1,1})} \\ &= 1 - \frac{1}{\mathbb{P}(\mathcal{E}_{1,1})} \mathbb{E}_{X_1} [\mathbb{P}(r_1 < D_1 < x_1|X_1)] \\ &= 1 - \frac{1}{\mathbb{P}(\mathcal{E}_{1,1})} \int_{r_1}^{\infty} (F_{D_1}(x_1) - F_{D_1}(r_1)) f_{X_1}(x_1) dx_1 \\ &= 1 - \frac{\lambda_l + \lambda_c}{\lambda_c} \int_{r_1}^{\infty} (e^{-\lambda_c r_1} - e^{-\lambda_c x_1}) \lambda_l e^{-\lambda_l x_1} dx_1 \\ &= 1 - \exp(-(\lambda_l + \lambda_c)r_1), \end{aligned}$$

where (a) follows from the condition for the occurrence of the event $\mathcal{E}_{1,1}$. ■

With this, we have derived all the intermediate results required to compute the CDF of R_1 . Combining these results given in Lemmas 2, 3, and 4, we will now derive the marginal CDF of R_1 in the following Lemma.

Lemma 5. *The CDF of R_1 is*

$$\begin{aligned} F_{R_1}(r_1) &= \int_{\frac{r_1}{2}}^{r_1} F_{W_1,1}(r_1 - x_1|\mathcal{E}_{0,1}, x_1) \mathbb{P}(\mathcal{E}_{0,1}|X_1) f_{X_1}(x_1) dx_1 \\ &+ \int_0^{\frac{r_1}{2}} F_{W_1,2}(r_1 - x_1|\mathcal{E}_{0,1}, x_1) \mathbb{P}(\mathcal{E}_{0,1}|X_1) f_{X_1}(x_1) dx_1 \\ &+ \mathbb{P}(\mathcal{E}_{1,1}) F_{R_1}(r_1|\mathcal{E}_{1,1}). \end{aligned} \quad (13)$$

Proof: The CDF of R_1 can be computed as

$$\begin{aligned} F_{R_1}(r_1) &= \mathbb{P}(R_1 < r_1) \\ &\stackrel{(a)}{=} \mathbb{P}(R_1 < r_1, \mathcal{E}_{0,1}) + \mathbb{P}(R_1 < r_1, \mathcal{E}_{1,1}) \\ &= \mathbb{E}_{X_1} [\mathbb{P}(R_1 < r_1, \mathcal{E}_{0,1}|X_1)] + \mathbb{P}(R_1 < r_1, \mathcal{E}_{1,1}) \\ &\stackrel{(b)}{=} \mathbb{E}_{X_1} [\mathbb{P}(R_1 < r_1|\mathcal{E}_{0,1}, X_1) \mathbb{P}(\mathcal{E}_{0,1}|X_1)] \\ &\quad + \mathbb{P}(R_1 < r_1|\mathcal{E}_{1,1}) \mathbb{P}(\mathcal{E}_{1,1}) \\ &= \int_0^{\infty} \mathbb{P}(x_1 + W_1 < r_1|\mathcal{E}_{0,1}, X_1) \mathbb{P}(\mathcal{E}_{0,1}|X_1) f_{X_1}(x_1) dx_1 \\ &\quad + \mathbb{P}(\mathcal{E}_{1,1}) \mathbb{P}(R_1 < r_1|\mathcal{E}_{1,1}) \\ &= \int_0^{\infty} F_{W_1}(r_1 - x_1|\mathcal{E}_{0,1}, x_1) \mathbb{P}(\mathcal{E}_{0,1}|X_1) f_{X_1}(x_1) dx_1 \\ &\quad + \mathbb{P}(\mathcal{E}_{1,1}) F_{R_1}(r_1|\mathcal{E}_{1,1}) \end{aligned}$$

$\lambda_l \backslash \lambda_c$	0.5	1	3	5
1	.0669	.0422	.0108	.0056
5	.0095	.0076	.0055	.0033
10	.0067	.0027	.0042	.0049

TABLE I: KL-divergence of the approximate joint PDF of R_1 and R_2 computed as the product of their marginal PDFs from their empirical joint PDF.

$$\begin{aligned}
&\stackrel{(c)}{=} \int_{\frac{r_1}{2}}^{r_1} F_{W_{1,1}}(r_1 - x_1 | \mathcal{E}_{0,1}, x_1) \mathbb{P}(\mathcal{E}_{0,1} | X_1) f_{X_1}(x_1) dx_1 \\
&+ \int_0^{\frac{r_1}{2}} F_{W_{1,2}}(r_1 - x_1 | \mathcal{E}_{0,1}, x_1) \mathbb{P}(\mathcal{E}_{0,1} | X_1) f_{X_1}(x_1) dx_1 \\
&+ \mathbb{P}(\mathcal{E}_{1,1}) F_{R_1}(r_1 | \mathcal{E}_{1,1}),
\end{aligned}$$

where (a) follows from the law of total probability, (b) follows from the application of Bayes' theorem, and (c) follows from substituting (9) in the previous step. ■

In order to compute the exact CDF of $\min\{R_1, R_2\}$, we need to determine the joint distribution of R_1 and R_2 , which is not quite tractable due to the peculiar coupling induced by the underlying line process. Therefore, in the interest of analytical tractability, we assume R_1 and R_2 to be independent and derive the approximate CDF of $\min\{R_1, R_2\}$. This assumption is strongly supported by the empirical evidence obtained from Monte-Carlo simulations. For different sets of λ_l and λ_c , we determined the Kullback-Leibler (KL) divergence of the approximate joint PDF of R_1 and R_2 computed as the product of their marginal PDFs from their actual joint PDF, as shown in Table I. It can be observed that the KL divergence for different combinations of λ_l and λ_c is quite small. Thus, we can infer that the dependence between R_1 and R_2 is minimal. So, using the assumption of independence between R_1 and R_2 , we derive an approximate lower bound for the CDF of R_m in the following theorem.

Theorem 2. For a typical general user, the CDF of R_m is approximately lower bounded by

$$F_{R_m}(r_m) \gtrsim 1 - (1 - F_{R_1}(r_m))^2, \quad (14)$$

where $F_{R_1}(\cdot)$ is the marginal distribution of R_1 given in Lemma 5.

Proof: The CDF of R_m can be computed as

$$\begin{aligned}
F_{R_m}(r_m) &= \mathbb{P}(R_m < r_m) \\
&\geq \mathbb{P}(\min\{R_1, R_2\} < r_m) \\
&= 1 - \mathbb{P}(R_1 > r_m, R_2 > r_m) \\
&\stackrel{(a)}{\approx} 1 - \mathbb{P}(R_1 > r_m) \mathbb{P}(R_2 > r_m) \\
&\stackrel{(b)}{=} 1 - (1 - F_{R_1}(r_m))^2,
\end{aligned}$$

where (a) follows from assuming R_1 and R_2 to be independent, and (b) follows from the identical distribution of R_1 and R_2 . This completes the proof. ■

V. RESULTS AND DISCUSSION

In the previous section, we have derived the analytical expressions for the CDF of the shortest path distance to the

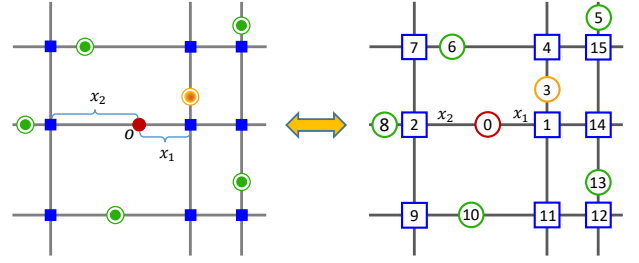


Fig. 9: Illustration of the equivalent weighted graph constructed from the spatial setup. The nodes corresponding to facilities are indicated by circles and the nodes corresponding to intersections are indicated by squares.

nearest facility for the typical intersection user and typical general user. We will focus on the computation of the empirical CDF of this distance and verification of our analytical results using Monte-Carlo simulations in this section. We will first present a simulation method to compute any distance-dependent metric using the spatial model described in Section III. We then verify the accuracy of analytical results by numerically comparing them with the results from Monte-Carlo simulations. We will also discuss the extension of this work to study other cost metrics in the context of various applications.

A. Simulation Techniques

In this subsection, we will present the procedure to characterize the minimum cost of travel for a typical vehicular user using Monte Carlo simulations. This method is applicable to any cost metric that depends on the spatial separation between the typical vehicular user and the facilities, such as path distance, travel time or fuel consumed. The problem of finding the minimum cost can be posed as a classical shortest path problem by interpreting the setup as a weighted graph where the weights of the edges correspond to the cost associated with traveling between those points.

In order to run Monte-Carlo simulations, we first generate a realization of the spatial model and calculate the cost of travel from the typical user (at origin) to all the facilities.

The next step is to construct an equivalent undirected weighted graph of the spatial setup, as illustrated in Fig. 9, by following these steps:

- The locations of the facilities, typical user, and the intersections of roads are considered as the nodes of a graph \mathcal{G} .
- Any two nodes of the graph are connected if and only if they are located on the same line and are also adjacent.
- The weight of an edge of the graph \mathcal{G} is equal to the cost incurred to travel between the points corresponding to the end points of the edge in \mathbb{R}^2 .

Now, we can easily find the minimum cost from the typical user (source node) to any facility (destination node) using *Dijkstra's algorithm* on the weighted graph, thereby eliminating the burden of determining all possible routes to a facility from the typical user [30]. We can then find the overall minimum cost to a facility by comparing the minimum cost of travel to

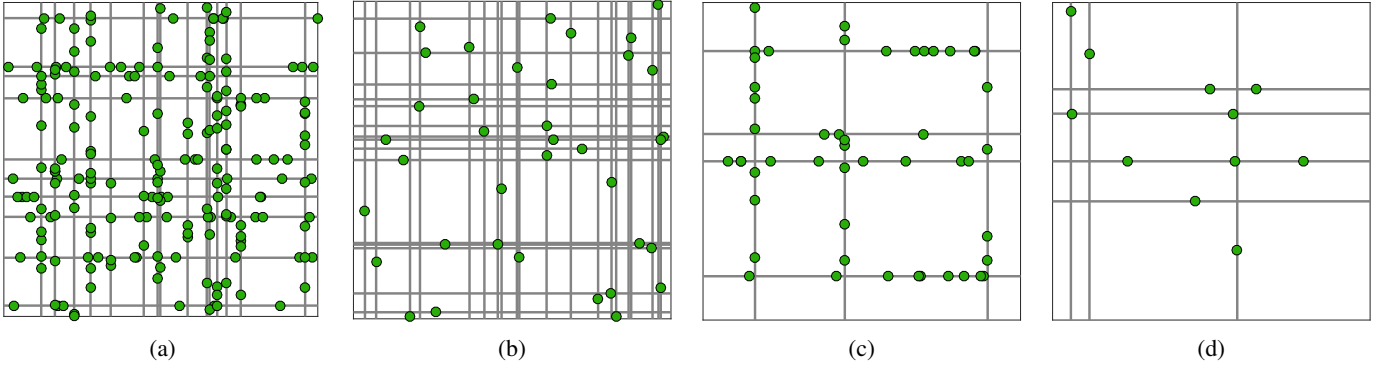


Fig. 10: The four different regimes of the spatial model: (a) Dense Roads-Dense Facilities (DR-DF), (b) Dense Roads-Sparse Facilities (DR-SF), (c) Sparse Roads-Dense Facilities (SR-DF), and (d) Sparse Roads-Sparse Facilities (SR-SF).

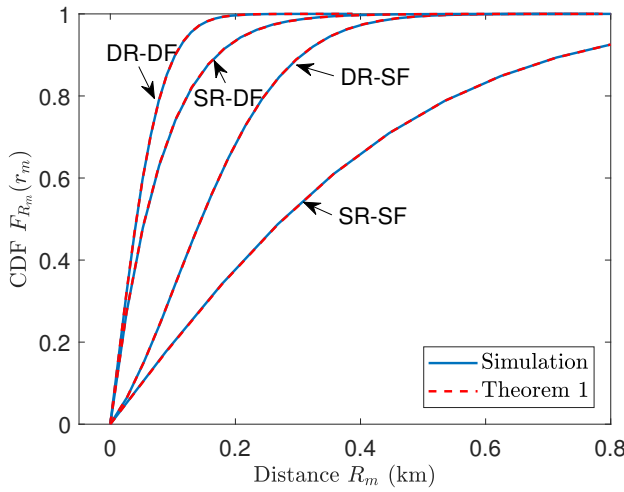


Fig. 11: CDF of the minimum shortest path distance for a typical intersection user for the four regimes: DR-DF ($\lambda_l = 10 \text{ km}^{-1}$, $\lambda_c = 3 \text{ facilities/km}$), SR-DF ($\lambda_l = 1 \text{ km}^{-1}$, $\lambda_c = 3 \text{ facilities/km}$), DR-SF ($\lambda_l = 10 \text{ km}^{-1}$, $\lambda_c = 0.5 \text{ facilities/km}$), and SR-SF ($\lambda_l = 1 \text{ km}^{-1}$, $\lambda_c = 0.5 \text{ facilities/km}$).

all the facilities in the spatial network. This process is repeated over several realizations of the spatial model to obtain an empirical CDF of the minimum travel cost between a typical user and a facility.

Remark 2. Although the Dijkstra's algorithm directly yields the shortest path to a destination node, it is still time consuming to apply the algorithm to every destination node. However, if the cost metric is the path distance, we can employ a simple strategy that would significantly reduce the run-time of simulations. Assuming that the shortest path distance to the nodes are determined sequentially, we first sort the destination nodes in the increasing order of their Euclidean distances from the origin. Then, we compute the shortest path distance to each destination node in that order by applying Dijkstra's algorithm until we encounter a destination node whose Euclidean distance E_i is greater than the shortest path distance M_j of any of the previous nodes, i.e., $E_i > \min\{M_1, M_2, \dots, M_{i-1}\}$. Thus, this technique will help in further reducing the computational load by avoiding the computation of the shortest path

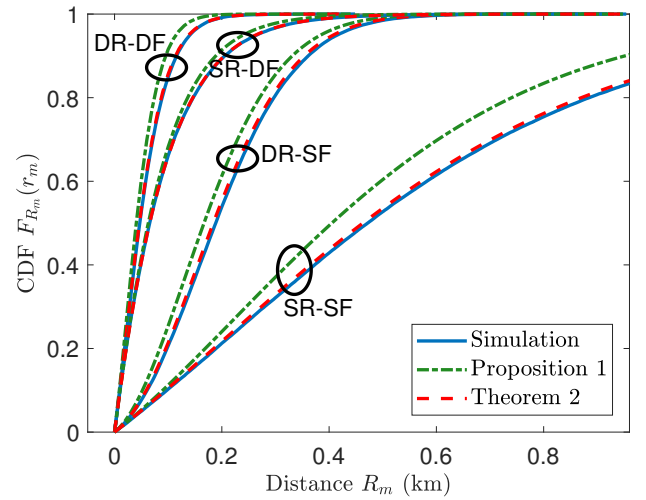


Fig. 12: CDF of the minimum shortest path distance for a typical general user for the four regimes: DR-DF ($\lambda_l = 10 \text{ km}^{-1}$, $\lambda_c = 5 \text{ facilities/km}$), SR-DF ($\lambda_l = 1 \text{ km}^{-1}$, $\lambda_c = 5 \text{ facilities/km}$), DR-SF ($\lambda_l = 10 \text{ km}^{-1}$, $\lambda_c = 0.5 \text{ facilities/km}$), and SR-SF ($\lambda_l = 1 \text{ km}^{-1}$, $\lambda_c = 0.5 \text{ facilities/km}$).

to every destination node.

B. Numerical Results

We first simulate the spatial model described in Section III in MATLAB. We then compute the empirical CDF of R_m and compare it with the CDF obtained from the analytical expressions given in Theorems 1 and 2. For exhaustive numerical analyses and comparisons, we define these four broad regimes based on the densities of roads and facilities: (i) Dense Roads-Dense Facilities (DR-DF) corresponding to large values of λ_l and λ_c , (ii) Dense Roads-Sparse Facilities (DR-SF) corresponding to large values of λ_l and small values of λ_c , (iii) Sparse Roads-Dense Facilities (SR-DF) corresponding to small values of λ_l and large values of λ_c , and (iv) Sparse Roads-Sparse Facilities (SR-SF) corresponding to small values of λ_l and λ_c , as illustrated in Fig. 10. Note that Fig. 10 is only for illustration purpose and the actual simulation values corresponding to these configurations are provided along with the results in Figs. 11 and 12. For a typical intersection

user, as expected, the CDF obtained from the expression in (1) matches exactly with the CDF obtained from Monte-Carlo simulations for all the configurations as depicted in Fig. 11. In case of a typical general user, while the upper bound given in Proposition 1 is not extremely tight in all the regimes, the approximate lower bound given in Theorem 2 closely follows the empirical CDF, as shown in Fig. 12. The remarkable accuracy of the lower bound follows from the careful construction of two approximately independent random variables R_1 and R_2 , as discussed in detail in Section IV.

C. Cost Metrics and Applications

In this section, we will discuss some of the other useful cost metrics related to transportation systems. We will also discuss the applicability and direct extensions of the results presented in this paper to address some of the problems related to infrastructure planning, personnel deployment and wireless communications.

1) *Transportation Systems*: Modeling spatial layout of roads as MPLP, we have comprehensively analyzed the shortest path distance between a typical vehicular user and its nearest facility in the sense of path distance. Some of the other metrics that could easily be studied are minimum travel time to a facility for a typical vehicular user and the fuel consumed to reach a facility. The minimum travel time to a facility can be computed as the sum of the ratios of length of each road segment along the path to the maximum speed permitted on the corresponding segment. Assuming that the maximum speed allowed u_{max} is the same on all the roads, the CDF of the minimum travel time to a facility T_m can be directly obtained from our analytical results as $F_{T_m}(t_m) = F_{R_m}(u_{max}t_m)$. For instance, assuming a speed limit of 40 km/hr, which is usually the case in downtown areas in major cities, we obtain the CDF for the minimum time of travel as shown in Fig. 13.

However, for an arbitrary distribution of velocities on different roads, the exact analysis is not straightforward. This is because the path that yields the shortest path distance to a facility is not necessarily the quickest path to reach a facility. However, we can obtain the lower bound for the minimum travel time by considering the same maximum velocity across all the roads. Similarly, we can obtain an upper bound on the minimum travel time by considering the same minimum velocity on all the roads. Our preliminary investigation indicates that these bounds may not be very tight and hence motivates future work in this direction. However, the simulation procedure presented in Section V-A is still valid and can be applied to compute the exact minimum travel time using Monte-Carlo simulations. In this case, the weight of an edge of the graph would be the minimum time taken to travel between the points corresponding to the end-points of the edge. Similarly, we could also characterize the fuel consumption of a typical vehicular user, as it is primarily a function of the distance traveled and the fuel efficiency of the vehicle.

2) *Infrastructure Planning/ Personnel Deployment*: As we have stated earlier in the paper, the facilities that we consider in our system model could be gas stations or other infrastructure.

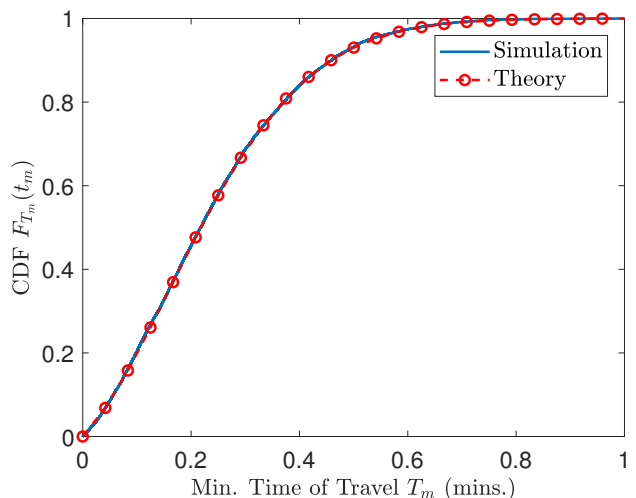


Fig. 13: CDF of the minimum travel time to a facility for a typical general user ($\lambda_l = 10 \text{ km}^{-1}$, $\lambda_c = 0.5 \text{ facilities/km}$, and $u_{max} = 40 \text{ km/hr}$).

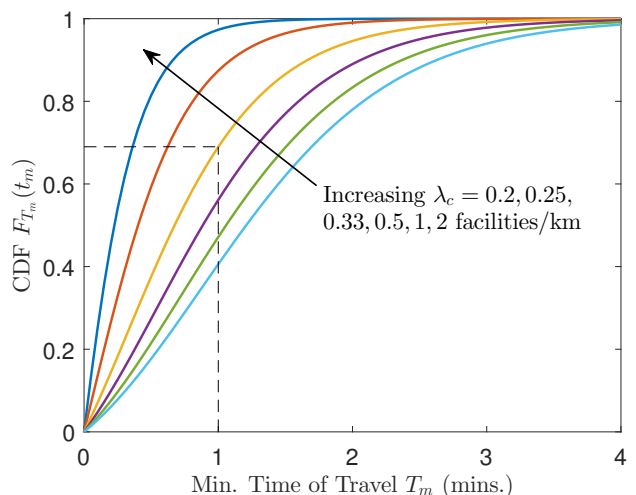


Fig. 14: CDF of the minimum travel time to a facility for a typical general user ($\lambda_l = 1 \text{ km}^{-1}$, and $u_{max} = 40 \text{ km/hr}$).

Using the analytical results presented in the paper, we can gain insights into the minimum distance to these facilities as a function of the density of roads and the density of facilities on each road. This would help in infrastructure planning to ensure that the minimum distance or minimum travel time to these facilities for a typical vehicular user does not exceed a desired threshold. For example, from Fig. 14 where we plot the CDF of minimum travel time for different values of the density of facilities, we can infer that the minimum travel time would be less than 1 minute with at least a probability of 70% if the value of λ_c is greater than 0.5 facilities/km. This analysis would be very useful in the study of the typical response time for first responders or police personnel to arrive at the site of an emergency or an accident.

3) *Wireless Communication*: The 5G New Radio (NR) standard for mobile communications includes the use of mmWave frequency spectrum (30 GHz - 300 GHz). Therefore, it is important to understand the performance of the network

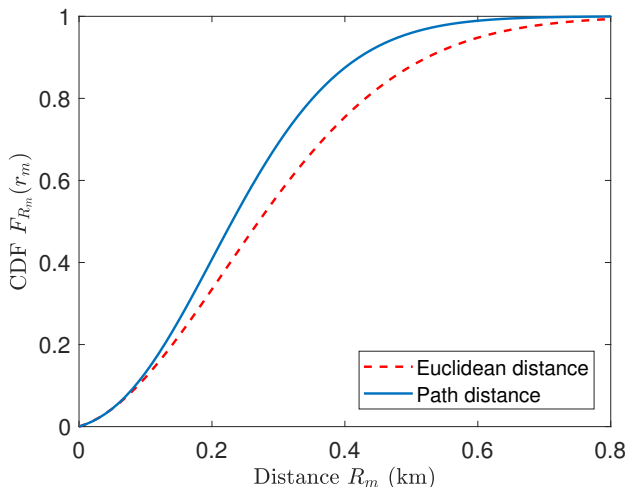


Fig. 15: CDF of the distance to the closest transmitting node in the sense of Euclidean distance and path distance ($\lambda_l = 10 \text{ km}^{-1}$, and $\lambda_c = 0.25 \text{ nodes/km}$).

at these higher frequencies. Unlike the cellular networks operating in sub-6 GHz frequencies, where the receiver usually connects to its closest transmitting node in the Euclidean distance sense, the propagation at higher frequencies is quite sensitive to blockages, thereby resulting in high attenuation of the signal. Therefore, in some urban scenarios with dense buildings and tall structures, it is quite possible that the dominant component of the received signal is the one that travels along the roads with diffraction around the corners at intersection [13]. Further, the strongest signal received from the desired transmitter is the one that travels along the shortest path. As is evident from Fig. 15, the CDF of the distance to the closest node in the Euclidean distance sense is significantly different from that of the closest node in the path distance sense. Therefore, the analytical techniques developed in this paper could be useful in characterizing the received signal power in such networks.

VI. CONCLUSION

Transportation systems have been mostly studied using spatial network models where various sites were modeled as nodes of a graph and the routes between those sites were modeled as edges of the graph. While these models are useful in studying the topological properties of the network, they do not accurately capture some of the geometric aspects such as continuity of streets. So, in this paper, we have modeled the spatial layout of roads by a MPLP and the locations of vehicles and facilities by independent and homogeneous 1D PPPs. For this setup, we first derived the closed-form expression for the CDF of the shortest path distance for a typical intersection user to its nearest facility in the sense of path distance. Building on this result, we derived an upper bound and a much tighter but approximate lower bound for the CDF of the shortest path distance for a typical general user. In addition to these analytical results, we also discussed a simulation method to characterize any distance-dependent metric through graphical interpretation of the spatial model.

We verified the accuracy of our analytical results by comparing them with the results obtained from Monte-Carlo simulations. We then discussed some key insights offered by our analytical results for infrastructure planning and personnel deployment.

This work has several extensions. First of all, the spatial model considered in the paper can be used to study other useful metrics such as route-length efficiency statistic which is defined as a function of the ratio of the shortest path distance between a pair of points to the corresponding Euclidean distance between those points [4]. While we have derived the results for an urban network by modeling the streets as a MPLP, the analytical procedure and the construction of bounds can be extended to a more general setup where the road network is modeled by a PLP. Another useful direction of work would be to explore the temporal behavior of the network by considering flow of vehicles along the streets modeled by a MPLP or a PLP. Also, the discussion on applications of our results in transportation, infrastructure planning, and wireless communication in Section V-C could motivate future work in all these areas.

APPENDIX

A. Proof of Theorem 1

The CDF of R_m can be computed as

$$\begin{aligned}
 F_{R_m}(r_m) &= 1 - \mathbb{P}(R_m > r_m) \\
 &= 1 - \mathbb{P}(N_p(\Phi_{l_0, \text{int}} \cap B_0) = 0) \\
 &\stackrel{(a)}{=} 1 - \mathbb{P}\left(N_p(\{L_x \cup \Phi_{lh}\} \cap B_0) = 0\right) \\
 &\quad \times \mathbb{P}\left(N_p(\{L_y \cup \Phi_{lv}\} \cap B_0) = 0\right) \\
 &\stackrel{(b)}{=} 1 - \left[\mathbb{P}(N_p(L_x \cap B_0) = 0) \sum_{n_{hl}=0}^{\infty} \mathbb{P}(N_h(B_0 \setminus L_x) = n_{hl}) \right. \\
 &\quad \times \mathbb{P}\left(N_p(\Phi_{lh} \cap B_0) = 0 | N_h(B_0 \setminus L_x) = n_{hl}\right) \Big] \\
 &\quad \times \left[\mathbb{P}(N_p(L_y \cap B_0) = 0) \sum_{n_{vl}=0}^{\infty} \mathbb{P}(N_v(B_0 \setminus L_y) = n_{vl}) \right. \\
 &\quad \times \mathbb{P}\left(N_p(\Phi_{lv} \cap B_0) = 0 | N_v(B_0 \setminus L_y) = n_{vl}\right) \Big] \\
 &\stackrel{(c)}{=} 1 - \left[\mathbb{P}(N_p(L_x \cap B_0) = 0) \sum_{n_{hl}=0}^{\infty} \mathbb{P}(N_h(B_0 \setminus L_x) = n_{hl}) \right. \\
 &\quad \times \left. \left(\prod_{j=1}^{n_{hl}} \mathbb{P}(N_p(L_{h_j} \cap B_0) = 0) \right) \right] \left[\mathbb{P}(N_p(L_y \cap B_0) = 0) \right. \\
 &\quad \times \left. \sum_{n_{vl}=0}^{\infty} \mathbb{P}(N_v(B_0 \setminus L_y) = n_{vl}) \left(\prod_{k=1}^{n_{vl}} \mathbb{P}(N_p(L_{v_k} \cap B_0) = 0) \right) \right] \\
 &\stackrel{(d)}{=} 1 - \left[e^{-2\lambda_c r_m} \sum_{n_{hl}=0}^{\infty} \frac{e^{-2\lambda_l r_m} (2\lambda_l r_m)^{n_{hl}}}{n_{hl}!} \right. \\
 &\quad \times \left. \left(\int_0^{r_m} \exp(-\lambda_c(2r_m - 2y)) \frac{dy}{r_m} \right)^{n_{hl}} \right] \\
 &\quad \times \left[e^{-2\lambda_c r_m} \sum_{n_{vl}=0}^{\infty} \frac{e^{-2\lambda_l r_m} (2\lambda_l r_m)^{n_{vl}}}{n_{vl}!} \right.
 \end{aligned}$$

$$\begin{aligned}
& \times \left[\int_0^{r_m} \exp(-\lambda_c(2r_m - 2x)) \frac{dx}{r_m} \right]^{n_{vl}} \\
& = 1 - \left[e^{-2\lambda_c r_m} e^{-2\lambda_l r_m} \exp \left[2\lambda_l \int_0^{r_m} e^{-2\lambda_c(r_m - y)} dy \right] \right] \\
& \quad \times \left[e^{-2\lambda_c r_m} e^{-2\lambda_l r_m} \exp \left[2\lambda_l \int_0^{r_m} e^{-2\lambda_c(r_m - x)} dx \right] \right] \\
& = 1 - \exp \left[-4\lambda_c r_m - 4\lambda_l r_m + \frac{2\lambda_l}{\lambda_c} (1 - e^{-2\lambda_c r_m}) \right],
\end{aligned}$$

where (a) follows from the fact that the distribution of horizontal and vertical lines are independent, (b) follows from conditioning on the number of horizontal and vertical lines intersecting the region B_0 , (c) follows from the independent distribution of facilities on the lines, and (d) follows from the Poisson distribution of the number of lines intersecting B_0 and the void probability of 1D PPP on each line.

B. Proof of Lemma 3

The conditional CDF of W_1 can be computed as

$$\begin{aligned}
F_{W_1}(w_1 | \mathcal{E}_{0,1}, x_1) & = 1 - \mathbb{P}(W_1 > w_1 | \mathcal{E}_{0,1}, X_1) \\
& = 1 - \mathbb{P}(N_p(B) = 0 | \mathcal{E}_{0,1}, X_1). \quad (15)
\end{aligned}$$

As we had discussed earlier, the shape of the exclusion zone B is different for the two cases $w_1 < x_1$ and $w_1 \geq x_1$ and hence we will handle these two cases separately. We will first consider the case $w_1 < x_1$. In this case, B is a square region and we now need to determine the probability that there are no points inside this square region centered at an intersection, as shown in Fig. 7. By expressing the conditional void probability in (15) as the product of void probabilities of independent individual components, as in the proof of Theorem 1, we obtain

$$\begin{aligned}
& \mathbb{P}(N_p(B) = 0 | \mathcal{E}_{0,1}, X_1) \\
& = \mathbb{P}(N_p(L_x \cap B) = 0 | \mathcal{E}_{0,1}, X_1) \\
& \quad \times \left[\sum_{n_{hl}=0}^{\infty} \mathbb{P}(N_h(B \setminus L_x) = n_{hl} | \mathcal{E}_{0,1}, X_1) \right. \\
& \quad \times \mathbb{P}(N_p(\Phi_{lh} \cap B) = 0 | N_h(B \setminus L_x) = n_{hl}, \mathcal{E}_{0,1}, X_1) \left. \right] \\
& \quad \times \mathbb{P}(N_p(L_{v_0} \cap B) = 0 | \mathcal{E}_{0,1}, X_1) \\
& \quad \times \left[\sum_{n_{vl}=0}^{\infty} \mathbb{P}(N_v(B_{x_1^+}) = n_{vl} | \mathcal{E}_{0,1}, X_1) \right. \\
& \quad \times \mathbb{P}(N_p(\Phi_{lv} \cap B_{x_1^+}) = 0 | N_v(B_{x_1^+}) = n_{vl}, \mathcal{E}_{0,1}, X_1) \left. \right] \\
& \stackrel{(a)}{=} \mathbb{P}(N_p(L_x \cap B) = 0 | \mathcal{E}_{0,1}, X_1) \\
& \quad \times \left[\sum_{n_{hl}=0}^{\infty} \mathbb{P}(N_h(B \setminus L_x) = n_{hl}) \right. \\
& \quad \times \mathbb{P}(N_p(\Phi_{lh} \cap B) = 0 | N_h(B \setminus L_x) = n_{hl}) \left. \right] \\
& \quad \times \mathbb{P}(N_p(L_{v_0} \cap B) = 0) \left[\sum_{n_{vl}=0}^{\infty} \mathbb{P}(N_v(B_{x_1^+}) = n_{vl}) \right.
\end{aligned}$$

$$\begin{aligned}
& \quad \times \mathbb{P}(N_p(\Phi_{lv} \cap B_{x_1^+}) = 0 | N_v(B_{x_1^+}) = n_{vl}) \left. \right] \\
& \stackrel{(b)}{=} \mathbb{P}(N_p(L_x \cap B) = 0 | \mathcal{E}_{0,1}, X_1) \\
& \quad \times \left[\sum_{n_{hl}=0}^{\infty} \mathbb{P}(N_h(B \setminus L_x) = n_{hl}) \right. \\
& \quad \times \left(\prod_{j=1}^{n_{hl}} \mathbb{P}(N_p(L_{h_j} \cap B) = 0) \right) \left. \right] \\
& \quad \times \mathbb{P}(N_p(L_{v_0} \cap B) = 0) \left[\sum_{n_{vl}=0}^{\infty} \mathbb{P}(N_v(B_{x_1^+}) = n_{vl}) \right. \\
& \quad \times \left(\prod_{k=1}^{n_{vl}} \mathbb{P}(N_p(L_{v_k} \cap B_{x_1^+}) = 0) \right) \left. \right] \\
& \stackrel{(c)}{=} e^{-\lambda_c w_1} \left[\sum_{n_{hl}=0}^{\infty} \frac{e^{-2\lambda_l w_1} (2\lambda_l w_1)^{n_{hl}}}{n_{hl}!} \right. \\
& \quad \times \left(\int_0^{w_1} \exp(-\lambda_c(2w_1 - 2y)) \frac{dy}{w_1} \right)^{n_{hl}} \left. \right] \\
& \quad \times e^{-2\lambda_c w_1} \left[\sum_{n_{vl}=0}^{\infty} \frac{e^{-\lambda_l w_1} (\lambda_l w_1)^{n_{vl}}}{n_{vl}!} \right. \\
& \quad \times \left(\int_0^{w_1} \exp(-\lambda_c(2w_1 - 2x)) \frac{dx}{w_1} \right)^{n_{vl}} \left. \right] \\
& = \left[e^{-\lambda_c w_1} e^{-2\lambda_l w_1} \exp \left[2\lambda_l \int_0^{w_1} e^{-2\lambda_c(w_1 - y)} dy \right] \right] \\
& \quad \times \left[e^{-2\lambda_c w_1} e^{-\lambda_l w_1} \exp \left[\lambda_l \int_0^{w_1} e^{-2\lambda_c(w_1 - x)} dx \right] \right] \\
& = \exp \left[-3\lambda_c w_1 - 3\lambda_l w_1 + \frac{3\lambda_l}{2\lambda_c} (1 - e^{-2\lambda_c w_1}) \right], \quad (16)
\end{aligned}$$

where (a) follows from the fact that the distribution of points on the random horizontal lines, random vertical lines intersecting $B_{x_1^+}$, and the line L_{v_0} is independent of $\mathcal{E}_{0,1}$ and X_1 , (b) follows from the independent distribution of points over different lines, and (c) follows from the Poisson distribution of lines and the void probability of 1D PPPs on those lines. Substituting (16) in (15), we obtain the expression for the conditional CDF of W_1 for the case $w_1 < x_1$.

We will now consider the case where $w_1 \geq x_1$, where the exclusion region B is a pentagon as depicted in Fig. 8. The length of the horizontal line segment inside B depends on the distance of the line from the origin. For a horizontal line L_h which intercepts the y -axis at y_h such that $|y_h| < w_1 - x_1$, the length of the line segment inside B is given by $x_1 + w_1 - |y_h|$. On the other hand, if $|y_h| \geq w_1 - x_1$, then the length of line segment inside B is $2(w_1 - |y_h|)$. So, we partition the set of horizontal lines that intersect B into two sets: (i) the set of horizontal lines that intersect the region $B_{h_1} = B \cap \{|y| < w_1 - x_1\}$, and (ii) the set of horizontal lines that intersect the region $B_{h_2} = B \cap \{|y| \geq w_1 - x_1\}$. As B_{h_2} is composed of two non-contiguous regions $B_{h_2^+} = B \cap \{y \geq w_1 - x_1\}$ and $B_{h_2^-} = B \cap \{y \leq -(w_1 - x_1)\}$, we will handle them separately in our analysis. Thus, the conditional void probability for the

case $w_1 \geq x_1$ can be computed as

$$\begin{aligned}
& \mathbb{P}(N_p(B) = 0 | \mathcal{E}_{0,1}, X_1) \\
&= \mathbb{P}(N_p(L_x \cap B) = 0 | \mathcal{E}_{0,1}, X_1) \\
&\times \left[\sum_{n_{h_1}=0}^{\infty} \mathbb{P}(N_h(B_{h_1} \setminus L_x) = n_{h_1} | \mathcal{E}_{0,1}, X_1) \right. \\
&\times \mathbb{P}(N_p(\Phi_{lh} \cap B_{h_1}) = 0 | N_h(B_{h_1} \setminus L_x) = n_{h_1}, \mathcal{E}_{0,1}, X_1) \left. \right] \\
&\times \left[\sum_{n_{h_2}=0}^{\infty} \mathbb{P}(N_h(B_{h_2}^+) = n_{h_2} | \mathcal{E}_{0,1}, X_1) \right. \\
&\times \mathbb{P}(N_p(\Phi_{lh} \cap B_{h_2}^+) = 0 | N_h(B_{h_2}^+) = n_{h_2}, \mathcal{E}_{0,1}, X_1) \\
&\times \sum_{n_{h_3}=0}^{\infty} \mathbb{P}(N_h(B_{h_2}^-) = n_{h_3} | \mathcal{E}_{0,1}, X_1) \\
&\times \mathbb{P}(N_p(\Phi_{lh} \cap B_{h_2}^-) = 0 | N_h(B_{h_2}^-) = n_{h_3}, \mathcal{E}_{0,1}, X_1) \left. \right] \\
&\times \mathbb{P}(N_p(L_{v_0} \cap B) = 0 | \mathcal{E}_{0,1}, X_1) \\
&\times \left[\sum_{n_{vl}=0}^{\infty} \mathbb{P}(N_v(B_{x_1}^+) = n_{vl} | \mathcal{E}_{0,1}, X_1) \right. \\
&\times \mathbb{P}(N_p(\Phi_{lv} \cap B_{x_1}^+) = 0 | N_v(B_{x_1}^+) = n_{vl}, \mathcal{E}_{0,1}, X_1) \left. \right] \\
&\stackrel{(a)}{=} \mathbb{P}(N_p(L_x \cap B) = 0 | \mathcal{E}_{0,1}, X_1) \mathbb{P}(N_p(L_{v_0} \cap B) = 0) \\
&\times \left[\sum_{n_{h_1}=0}^{\infty} \mathbb{P}(N_h(B_{h_1} \setminus L_x) = n_{h_1} | X_1) \right. \\
&\times \mathbb{P}(N_p(\Phi_{lh} \cap B_{h_1}) = 0 | N_h(B_{h_1} \setminus L_x) = n_{h_1}, X_1) \left. \right] \\
&\times \left[\sum_{n_{h_2}=0}^{\infty} \mathbb{P}(N_h(B_{h_2}^+) = n_{h_2} | X_1) \right. \\
&\times \mathbb{P}(N_p(\Phi_{lh} \cap B_{h_2}^+) = 0 | N_h(B_{h_2}^+) = n_{h_2}, X_1) \\
&\times \sum_{n_{h_3}=0}^{\infty} \mathbb{P}(N_h(B_{h_2}^-) = n_{h_3} | X_1) \\
&\times \mathbb{P}(N_p(\Phi_{lh} \cap B_{h_2}^-) = 0 | N_h(B_{h_2}^-) = n_{h_3}, X_1) \left. \right] \\
&\times \left[\sum_{n_{vl}=0}^{\infty} \mathbb{P}(N_v(B_{x_1}^+) = n_{vl} | X_1) \right. \\
&\times \mathbb{P}(N_p(\Phi_{lv} \cap B_{x_1}^+) = 0 | N_v(B_{x_1}^+) = n_{vl}, X_1) \left. \right], \\
&\stackrel{(b)}{=} \mathbb{P}(N_p(L_x \cap B) = 0 | \mathcal{E}_{0,1}, X_1) \mathbb{P}(N_p(L_{v_0} \cap B) = 0) \\
&\times \left[\sum_{n_{h_1}=0}^{\infty} \mathbb{P}(N_h(B_{h_1} \setminus L_x) = n_{h_1} | X_1) \right. \\
&\quad \times \left(\prod_{i=1}^{n_{h_1}} \mathbb{P}(N_p(L_{h_i} \cap B_{h_1}) = 0 | X_1) \right) \left. \right] \\
&\times \left[\sum_{n_{h_2}=0}^{\infty} \mathbb{P}(N_h(B_{h_2}^+) = n_{h_2} | X_1) \right. \\
&\quad \times \left(\prod_{j=1}^{n_{h_2}} \mathbb{P}(N_p(L_{h_j} \cap B_{h_2}^+) = 0 | X_1) \right) \left. \right] \\
&\times \left[\sum_{n_{h_3}=0}^{\infty} \mathbb{P}(N_h(B_{h_2}^-) = n_{h_3} | X_1) \right. \\
&\quad \times \left(\prod_{j=1}^{n_{h_3}} \mathbb{P}(N_p(L_{h_j} \cap B_{h_2}^-) = 0 | X_1) \right) \left. \right] \\
&\times \left[\sum_{n_{vl}=0}^{\infty} \mathbb{P}(N_v(B_{x_1}^+) = n_{vl} | X_1) \right. \\
&\quad \times \left(\prod_{k=1}^{n_{vl}} \mathbb{P}(N_p(L_{v_k} \cap B_{x_1}^+) = 0) \right) \left. \right] \\
&\stackrel{(c)}{=} e^{-\lambda_c(w_1+x_1)} e^{-2\lambda_c w_1} \\
&\times \left[\sum_{n_{h_1}=0}^{\infty} \frac{e^{-2\lambda_l(w_1-x_1)} (2\lambda_l(w_1-x_1))^{n_{h_1}}}{n_{h_1}!} \right. \\
&\times \left(\int_0^{w_1-x_1} \exp(-\lambda_c(x_1+w_1-y)) \frac{dy}{(w_1-x_1)} \right)^{n_{h_1}} \left. \right] \\
&\times \left[\sum_{n_{h_2}=0}^{\infty} \frac{e^{-\lambda_l x_1} (\lambda_l x_1)^{n_{h_2}}}{n_{h_2}!} \left(\int_{w_1-x_1}^{w_1} e^{-\lambda_c(2w_1-2y)} \frac{dy}{x_1} \right)^{n_{h_2}} \right. \\
&\times \sum_{n_{h_3}=0}^{\infty} \frac{e^{-\lambda_l x_1} (\lambda_l x_1)^{n_{h_3}}}{n_{h_3}!} \left(\int_{w_1-x_1}^{w_1} e^{-\lambda_c(2w_1-2y)} \frac{dy}{x_1} \right)^{n_{h_3}} \left. \right] \\
&\times \left[\sum_{n_{vl}=0}^{\infty} \frac{e^{-\lambda_l w_1} (\lambda_l w_1)^{n_{vl}}}{n_{vl}!} \left(\int_0^{w_1} e^{-\lambda_c(2w_1-2x)} \frac{dx}{w_1} \right)^{n_{vl}} \right. \\
&= \exp \left[-3(\lambda_c + \lambda_l)w_1 - \lambda_c x_1 + \frac{\lambda_l}{2\lambda_c} (3 + 2e^{-2\lambda_c x_1} \right. \\
&\quad \left. - e^{-2\lambda_c w_1} - 4e^{-\lambda_c(x_1+w_1)}) \right], \quad (17)
\end{aligned}$$

where (a) follows from the fact that the distribution of points on the random horizontal lines, vertical lines intersecting $B_{x_1}^+$ and the line L_{v_0} are independent of $\mathcal{E}_{0,1}$, (b) follows from the independent distribution of points over lines, and (c) follows from the Poisson distribution of lines and the void probability of 1D PPPs on each of those lines. Substituting (17) in (15), we obtain the expression for the conditional CDF of W_1 for the case $w_1 \geq x_1$. This completes the proof.

REFERENCES

- [1] J. Lin, "Spatial analysis and modelling of urban transportation networks," Ph.D. dissertation, KTH Royal Institute of Technology, 2017.
- [2] S. Marshall, J. Gil, K. Kropf, M. Tomko, and L. Figueiredo, "Street network studies: from networks to models and their representations," *Networks and Spatial Economics*, pp. 1–15, 2018.
- [3] M. Barthélemy, "Spatial networks," *Physics Reports*, vol. 499, no. 1–3, pp. 1–101, 2011.
- [4] D. J. Aldous and J. Shun, "Connected spatial networks over random points and a route-length statistic," *Statist. Sci.*, vol. 25, no. 3, pp. 275–288, Aug. 2010.
- [5] C. P. Dettmann, O. Georgiou, and P. Pratt, "Spatial networks with wireless applications," *Comptes Rendus Physique*, vol. 19, no. 4, pp. 187–204, 2018.
- [6] S. Marshall, "Line structure representation for road network analysis," *Journal of Transport and Land Use*, vol. 9, no. 1, 2015.

- [7] F. Baccelli, M. Klein, M. Lebourges, and S. Zuyev, "Stochastic geometry and architecture of communication networks," *Telecommunication Systems*, vol. 7, no. 1, pp. 209–227, Jun. 1997.
- [8] C. Gloaguen, F. Fleischer, H. Schmidt, and V. Schmidt, "Analysis of shortest paths and subscriber line lengths in telecommunication access networks," *Networks and Spatial Economics*, vol. 10, no. 1, pp. 15–47, Mar. 2010.
- [9] V. V. Chetlur and H. S. Dhillon, "Coverage analysis of a vehicular network modeled as Cox process driven by poisson line process," *IEEE Trans. on Wireless Commun.*, to appear.
- [10] S. N. Chiu, D. Stoyan, W. S. Kendall, and J. Mecke, *Stochastic geometry and its applications*. John Wiley & Sons, 2013.
- [11] R. E. Miles, "Random polygons determined by random lines in a plane," *Proceedings of the National Academy of Sciences*, vol. 52, no. 4, pp. 901–907, 1964.
- [12] C. Choi and F. Baccelli, "Poisson Cox point processes for vehicular networks," *IEEE Trans. on Veh. Technology*, vol. 67, no. 10, pp. 10 160–10 165, Oct. 2018.
- [13] Y. Wang, K. Venugopal, R. W. Heath, and A. F. Molisch, "Mmwave vehicle-to-infrastructure communication: Analysis of urban microcellular networks," *IEEE Trans. on Veh. Technology*, 2018.
- [14] M. Haenggi, *Stochastic Geometry for Wireless Networks*. Cambridge University Press, 2013.
- [15] V. V. Chetlur and H. S. Dhillon, "Downlink coverage analysis for a finite 3D wireless network of unmanned aerial vehicles," *IEEE Trans. on Commun.*, to appear.
- [16] P. Erdős and A. Rényi, "On random graphs, I," *Publicationes Mathematicae (Debrecen)*, vol. 6, pp. 290–297, 1959.
- [17] —, "On the evolution of random graphs," in *Publication of the Mathematical Inst. of the Hungarian Acad. of Sci.*, 1960, pp. 17–61.
- [18] R. Albert and A.-L. Barabási, "Statistical mechanics of complex networks," *Rev. Mod. Phys.*, vol. 74, pp. 47–97, Jan 2002.
- [19] D. J. Watts and S. H. Strogatz, "Collective dynamics of 'small-world' networks," *nature*, vol. 393, no. 6684, p. 440, 1998.
- [20] D. Aldous and P. Diaconis, "Hammersley's interacting particle process and longest increasing subsequences," *Probability Theory and Related Fields*, vol. 103, no. 2, pp. 199–213, Jun. 1995.
- [21] F. Voss, C. Gloaguen, F. Fleischer, and V. Schmidt, "Distributional properties of Euclidean distances in wireless networks involving road systems," *IEEE Journal on Sel. Areas in Commun.*, vol. 27, no. 7, pp. 1047–1055, Sep. 2009.
- [22] C. Gloaguen, F. Fleischer, H. Schmidt, and V. Schmidt, "Simulation of typical Cox Voronoi cells with a special regard to implementation tests," *Mathematical Methods of Operations Research*, vol. 62, no. 3, pp. 357–373, 2005.
- [23] —, "Fitting of stochastic telecommunication network models via distance measures and Monte-Carlo tests," *Telecommunication Systems*, vol. 31, no. 4, pp. 353–377, Apr. 2006.
- [24] V. V. Chetlur and H. S. Dhillon, "Success probability and area spectral efficiency of a VANET modeled as a Cox process," *IEEE Wireless Commun. Letters*, vol. 7, no. 5, pp. 856–859, Oct. 2018.
- [25] C. Choi and F. Baccelli, "An analytical framework for coverage in cellular networks leveraging vehicles," *IEEE Transactions on Communications*, vol. 66, no. 10, pp. 4950–4964, Oct. 2018.
- [26] F. Baccelli and X. Zhang, "A correlated shadowing model for urban wireless networks," in *Proc., IEEE INFOCOM*. IEEE, 2015, pp. 801–809.
- [27] X. Zhang, F. Baccelli, and R. W. Heath, "An indoor correlated shadowing model," in *Proc., IEEE Globecom*, 2015, pp. 1–7.
- [28] 3GPP TR 36.885, "Study on LTE-based V2X services," Jul. 2016.
- [29] F. Morlot, "A population model based on a Poisson line tessellation," in *Proc., Modeling and Optimization in Mobile, Ad Hoc and Wireless Networks*, May 2012, pp. 337–342.
- [30] E. W. Dijkstra, "A note on two problems in connexion with graphs," *Numerische mathematik*, vol. 1, no. 1, pp. 269–271, 1959.



Vishnu Vardhan Chetlur received the B. E. (Hons.) degree in Electronics and Communications Engineering from the Birla Institute of Technology and Science (BITS) Pilani, India, in 2013. After his graduation, he worked as a design engineer at Redpine Signals Inc. for two years. He is currently a Ph.D. student at Virginia Tech, where his research interests include wireless communication, smart cities, and stochastic geometry. He has held short-term visiting positions at Bell Labs, Qualcomm Inc., and Philips Research India. He graduated top of his class in the department of Electrical Engineering at BITS and was awarded the institute Silver medal for being ranked second in the whole institute. He was also a recipient of the BITS merit scholarship for his excellence in academics.



Harpreet S. Dhillon (S'11–M'13) received the B.Tech. degree in Electronics and Communication Engineering from IIT Guwahati, India, in 2008; the M.S. degree in Electrical Engineering from Virginia Tech, Blacksburg, VA, USA, in 2010; and the Ph.D. degree in Electrical Engineering from the University of Texas at Austin, TX, USA, in 2013. In academic year 2013–14, he was a Viterbi Postdoctoral Fellow at the University of Southern California, Los Angeles, CA, USA. He joined Virginia Tech in August 2014, where he is currently an Assistant Professor

and Steven O. Lane Junior Faculty Fellow of Electrical and Computer Engineering. He has held short-term visiting positions at Bell Labs, Samsung Research America, Qualcomm Inc., and Politecnico di Torino. His research interests include communication theory, stochastic geometry, geolocation, and wireless *ad hoc* and heterogeneous cellular networks.

Dr. Dhillon is a Clarivate Analytics Highly Cited Researcher and has coauthored five best paper award recipients including the 2016 IEEE Communications Society (ComSoc) Heinrich Hertz Award, the 2015 IEEE ComSoc Young Author Best Paper Award, the 2014 IEEE ComSoc Leonard G. Abraham Prize, and two conference best paper awards at IEEE ICC 2013 and European Wireless 2014. He was named the 2018 College of Engineering Faculty Fellow and the 2017 Outstanding New Assistant Professor by Virginia Tech. His other academic honors include the 2013 UT Austin Wireless Networking and Communications Group (WNCG) leadership award, the UT Austin Microelectronics and Computer Development (MCD) Fellowship, and the 2008 Agilent Engineering and Technology Award. He currently serves as an Editor for the IEEE TRANSACTIONS ON WIRELESS COMMUNICATIONS, the IEEE TRANSACTIONS ON GREEN COMMUNICATIONS AND NETWORKING, and the IEEE WIRELESS COMMUNICATIONS LETTERS.



Carl P. Dettmann received the BSc (Hons.) and the PhD degrees in physics from the University of Melbourne, Australia, in 1991 and 1995, respectively. Following research positions at New South Wales, Northwestern, Copenhagen, and Rockefeller Universities, he moved to the University of Bristol, Bristol, United Kingdom, where he is now professor and deputy director of the Institute of Probability, Analysis, and Dynamics. He has published more than 125 international journal and conference papers in complex and communications networks, dynamical systems, and statistical physics. He is a Fellow of the Institute of Physics and serves on its fellowship panel. He has delivered many presentations at international conferences, including a plenary lecture at Dynamics Days Europe and a tutorial at the International Symposium on Wireless Communication Systems.